Editors' Suggestion   Featured in Physics

Formation and Stability of Dense Methane-Hydrogen Compounds

Umbertoluca Ranieri[1,2] Lewis J. Conway,[3] Mary-Ellen Donnelly,[1] Huixin Hu,[1] Mengnan Wang,[1]
Philip Dalladay-Simpson,[1] Miriam Peña-Alvarez,[3] Eugene Gregoryanz,[1,3,4] Andreas Hermann,[3] and Ross T. Howie[1,3,*]

[1]*Center for High Pressure Science and Technology Advanced Research, 1690 Cailun Road, Shanghai, 201203, China*
[2]*Dipartimento di Fisica, Università di Roma La Sapienza, Piazzale Aldo Moro 5, 00185 Rome, Italy*
[3]*Centre for Science at Extreme Conditions and The School of Physics and Astronomy, The University of Edinburgh,*
Peter Guthrie Tait Road, Edinburgh, United Kingdom
[4]*Key Laboratory of Materials Physics, Institute of Solid State Physics, CAS, Hefei, China*

Through a series of x-ray diffraction, optical spectroscopy diamond anvil cell experiments, combined with density functional theory calculations, we explore the dense CH_4-H_2 system. We find that pressures as low as 4.8 GPa can stabilize $CH_4(H_2)_2$ and $(CH_4)_2H_2$, with the latter exhibiting extreme hardening of the intramolecular vibrational mode of H_2 units within the structure. On further compression, a unique structural composition, $(CH_4)_3(H_2)_{25}$, emerges. This novel structure holds a vast amount of molecular hydrogen and represents the first compound to surpass 50 wt % H_2. These compounds, stabilized by nuclear quantum effects, persist over a broad pressure regime, exceeding 160 GPa.

Hydrogen and methane are, besides water, the most prevalent small molecules in the outer Solar System. Their interplay under extreme conditions is of key interest to understanding the evolution and interior dynamics of Neptune and Uranus, as well as of Earth and exoplanets [1–4]. The simplest molecule, H_2, has been shown to exhibit rich physical phenomena, including quantum rotational phases and pressure-induced steps toward an atomic metallic solid, while methane (CH_4), the simplest hydrocarbon, has been proposed to polymerize during compression to form long-chain hydrocarbons and at further extremes decompose into diamond plus H_2 [5–19].

Hydrogen reacts with a number of materials at high pressures and temperatures but also has a propensity to form van der Waals compounds that can be stable far beyond 100 GPa [20–32]. Methane and hydrogen were first reported to crystallize into inclusion (host-guest) compounds over 25 years ago at pressures between 5 and 7 GPa. A range of compositions were claimed: $(CH_4)_2H_2$, CH_4H_2, $CH_4(H_2)_2$, and $CH_4(H_2)_4$ [21]. However, the experimental evidence for these compounds was limited, with only the shift of the hydrogen intramolecular vibrational mode ν_1-H_2 (vibron) relative to that of pure hydrogen being reported together with the lattice parameters of potential structures. Assuming that these structural compositions were correct, a later experimental study explored the recoverability of $CH_4(H_2)_4$ at low temperature to investigate its potential as a hydrogen storage media [33,34].

In contrast to experimental work, the CH_4-H_2 system has recently had a surge of theoretical investigations, predicting a variety of extremely hydrogen-rich compositions to emerge such as triclinic $(CH_4)_2(H_2)_3$, trigonal $(CH_4)_2(H_2)_7$, and

hexagonal $CH_4(H_2)_9$, as well as several CH_4H_2 structures [18,35–37]. Furthermore, it was suggested that CH_4-H_2 structures could be the most stable form of carbon and hydrogen at pressures up to 200 GPa [18].

Surprisingly, given these predictions and the advent of technological advances over the past 25 years, no further experimental exploration has been conducted despite undetermined CH_4-H_2 compound signatures emerging as a by-product in many prolific studies of hydrocarbons at planetary conditions [3,19,38–41]. Moreover, the doping of carbon (or methane) could even enhance the properties of materials at extreme pressures, with the unprecedented claim of room temperature superconductivity in the carbonaceous sulfur hydride system [42–44]. The lack of knowledge regarding CH_4-H_2 compound formation inhibits our understanding of these more complex ternary systems and how doping could induce novel properties. As such, it is of fundamental interest to know which methane-hydrogen compounds are actually formed and test their pressure stability limits.

In this Letter, we have conducted a series of high-pressure synchrotron powder x-ray diffraction and Raman spectroscopy experiments in diamond anvil cells combined with density functional theory (DFT) calculations and structural searching to explore the formation and properties of CH_4-H_2 compounds from mixtures of methane and hydrogen. In H_2-rich mixtures, we observe the formation of hexagonal $CH_4(H_2)_2$ above 5 GPa, before partially transforming into monoclinic $(CH_4)_3(H_2)_{25}$. $(CH_4)_3(H_2)_{25}$ represents a unique composition and contains an unprecedented 51.1 wt % H_2, which is the highest hydrogen content of any currently known
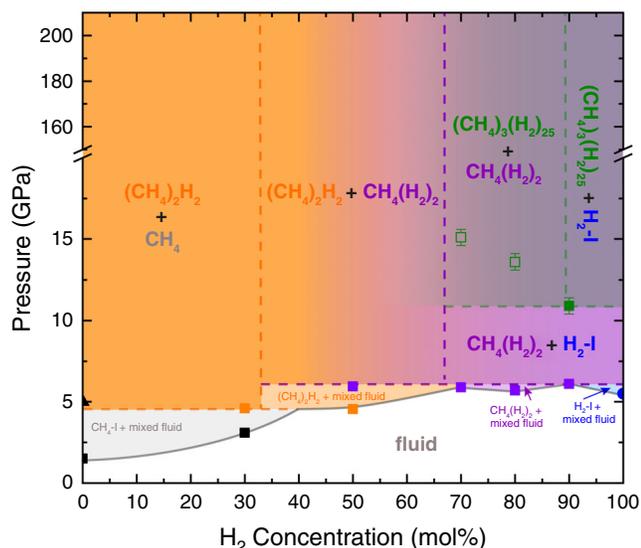
FIG. 1. Pressure-composition phase diagram of the CH_4-H_2 binary system. Filled square symbols indicate the formation pressures of each compound: $(CH_4)_2H_2$ (orange), $CH_4(H_2)_2$ (purple), and $(CH_4)_3(H_2)_{25}$ (green). The green open squares represent the pressures at which $(CH_4)_3(H_2)_{25}$ is first observed. The black squares, black triangle, and blue circle represent the formation pressure of CH_4-I, CH_4-A, and H_2-I, respectively. The gray line represents the liquidus curve and is adapted from Ref. [21]. Below 7 GPa, the error in pressure is ± 0.2 GPa and smaller than the size of the symbol. Initial gas mixtures have a tolerance of 1%.

stoichiometric compound. In CH_4-rich mixtures, tetragonal $(CH_4)_2H_2$ forms, which undergoes extreme hardening of the H_2 intramolecular vibrational mode with pressure. All three compounds exhibit remarkable stability, exceeding pressures of 160 GPa.

At pressures below 1.5 GPa, all mixture concentrations (30, 50, 70, 80, and 90 mol % H_2) are homogeneous well-mixed fluids and display the Raman signatures of both constituent species (see Fig. 1 for the pressure-composition phase diagram, Supplemental Material [45] for experimental methods, and Figs. S1–S9 [45] for Raman spectra of all mixtures). On compression of hydrogen-rich CH_4-H_2 mixtures (70–90 mol % H_2) above 5 GPa, the fluid mixture crystallizes into a solid which we identify as $CH_4(H_2)_2$. X-ray diffraction measurements reveal that this compound adopts a hexagonal $MgZn_2$ Laves phase structure (space group $P6_3/mmc$), where the CH_4 molecules occupy the Mg sites and the H_2 molecules occupy the Zn sites (see Fig. 2), the lattice parameters of which are $a = 4.981$ Å and $c = 8.125$ Å at 16.6 GPa. This structure and composition was suggested previously but attributed to a compound forming in a narrow pressure regime (between approximately 6 and 7 GPa) and between 35 and 65 mol % H_2 mixture concentrations [21]. Here, we find that $CH_4(H_2)_2$ is the dominant phase across all H_2-rich mixtures and persistent over a large pressure regime. Raman spectroscopy

reveals two distinct H_2 vibrons, ν_{1H} and ν_{2H}, the latter of which is approximately 50 times lower in intensity. The two most intense CH_4 stretching modes, ν_{1M} and ν_{2M}, are shifted to higher frequency compared to pure CH_4, while the wagging mode is shifted to lower frequency (see Figs. 3 and 4).

On further compression, we observe another compound emerge evidenced by visual changes in the sample morphology and the appearance of three distinct H_2 vibrational modes (the lowest in frequency being the most intense by 2 orders of magnitude) and CH_4 stretching bands that can be isolated from $CH_4(H_2)_2$ (see Figs. 3 and 4 and Supplemental Material [45]). The most intense H_2 vibron is lower in frequency than that of $CH_4(H_2)_2$, suggestive that the compound has a higher H_2 content. X-ray diffraction measurements indicate the compound is weakly scattering; however, this could be in part due to only partial transformation of the sample. The patterns could be indexed to a hexagonal cell, with $a = 7.804$ Å and $c = 11.199$ Å at 17.3 GPa (see Fig. 2). Systematic absences, unit cell volume, and c/a ratio suggest this compound has a close resemblance with the previously reported $R\bar{3}m$ structure of $Xe(H_2)_8$ [23,26] and an initial composition estimate of $CH_4(H_2)_8$. This seemed plausible given CH_4 and Xe have similar van der Waals diameters (3.78 and 4.32 Å, respectively).

We subsequently performed DFT calculations to help identify this phase. We constructed a series of structures of variable composition, starting by populating the hexagonal cell with randomly oriented CH_4 molecules on the Xe sites of $Xe(H_2)_8$, before adding H_2 molecules on hexagonal close packed (hcp) arrangements commensurate with the cell, using up to $3 \times 3 \times 4$ repeats of the hcp lattice and a random offset against the CH_4 sublattice. H_2 molecules too close to CH_4 were removed before fully optimizing the remaining atoms and all lattice parameters. Several thousand of these structures were generated with stoichiometries ranging from $CH_4(H_2)_7$ to $CH_4(H_2)_{11}$. Of these, $CH_4(H_2)_{8.33}$ [or $(CH_4)_3(H_2)_{25}$] emerged as the most energetically competitive and was found to be dynamically stable at and above 20 GPa (see Figs. S20 and S21 [45]). It is also the only computationally obtained structure which reproduces the positions and intensities of the experimental diffraction peaks across the studied pressure range (see Fig. S14 [45]), which is meaningful given that no symmetry restrictions were applied in the structures' construction and subsequent optimization. While we find both $CH_4(H_2)_2$ and $(CH_4)_2H_2$ stable or close to stability within the CH_4-H_2 phase diagram across a wide pressure range, once zero point energies and vibrational entropies are accounted for, $(CH_4)_3(H_2)_{25}$ remains metastable throughout (see Supplemental Material [45]).

Considering methane and hydrogen molecules to be spherical, the structure of $(CH_4)_3(H_2)_{25}$ is monoclinic with space group $C2/m$ (coordinates are given in Supplemental
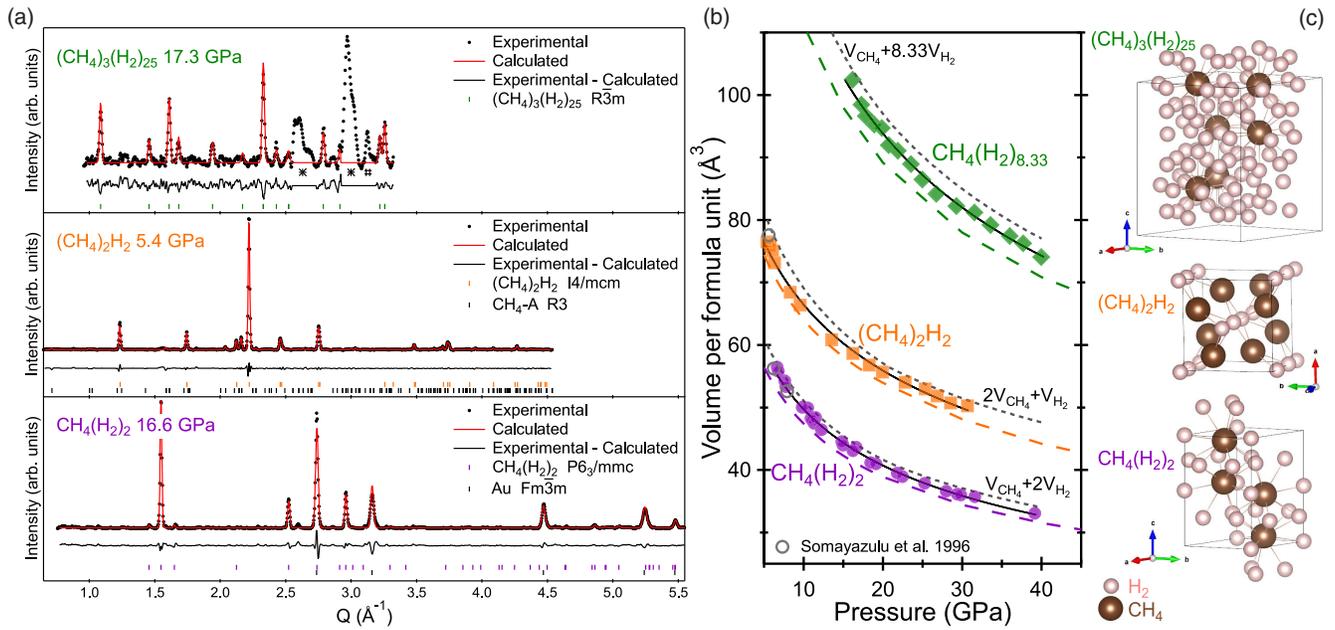
FIG. 2. (a) Representative x-ray diffraction patterns of the three compounds plotted as a function of exchanged wave vector and their Le Bail refinements. Refinements include $(CH_4)_3(H_2)_{25}$-$R\overline{3}m$ ($a = 7.804$ Å and $c = 11.199$ Å), $(CH_4)_2H_2$-$I4/mcm$ ($a = 7.195$ Å and $c = 5.909$ Å), CH_4-A-$R3$ ($a = 12.306$ Å and $c = 15.520$ Å), $CH_4(H_2)_2$-$P6_3/mmc$ ($a = 4.981$ Å and $c = 8.125$ Å), and Au-$Fm\overline{3}m$ ($a = 3.976$ Å). Excluded regions in the pattern of $(CH_4)_3(H_2)_{25}$ correspond to rhenium (gasket material) and rhenium hydride (*) and excess H_2 (#). (b) Volumes per formula unit as a function of pressure. Symbols represent experimental data (the error bars are smaller than the symbol size), and black full lines represent their best second-order Birch-Murnaghan fits: $CH_4(H_2)_{8.33}$, $V_0 = 246 \pm 17$ Å^3 and $K = 3.0 \pm 0.6$ GPa; $(CH_4)_2H_2$, $V_0 = 101 \pm 2$ Å^3 and $K = 10.2 \pm 0.8$ GPa; $CH_4(H_2)_2$, $V_0 = 90 \pm 3$ Å^3 and $K = 5.0 \pm 0.4$ GPa. Dashed lines represent volumes derived from our DFT calculations, and gray dotted lines represent the volumes of ideal mixtures of CH_4-A/CH_4-B and H_2-I using the previously determined equations of state [14,17,69]. The experimental volumes given in Ref. [21] are represented by gray circles. (c) Structural models of the three compounds, where CH_4 and H_2 are represented by brown and white spheres, respectively, and lines indicate CH_4-H_2 nearest neighbors.
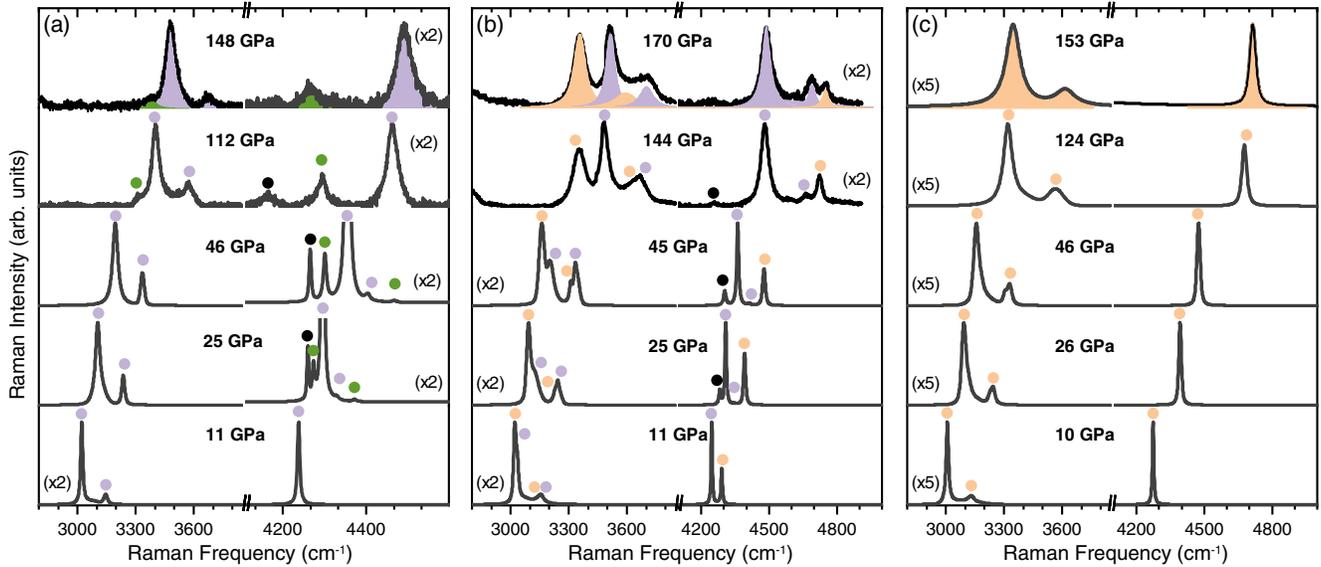

FIG. 3. Representative vibrational Raman spectra of (a) 70% H_2, (b) 50% H_2, and (c) 30% H_2 mixtures. Colors indicate the modes assigned to $CH_4(H_2)_2$ (purple), $(CH_4)_3(H_2)_{25}$ (green), $(CH_4)_2H_2$ (orange), and excess H_2 (black).
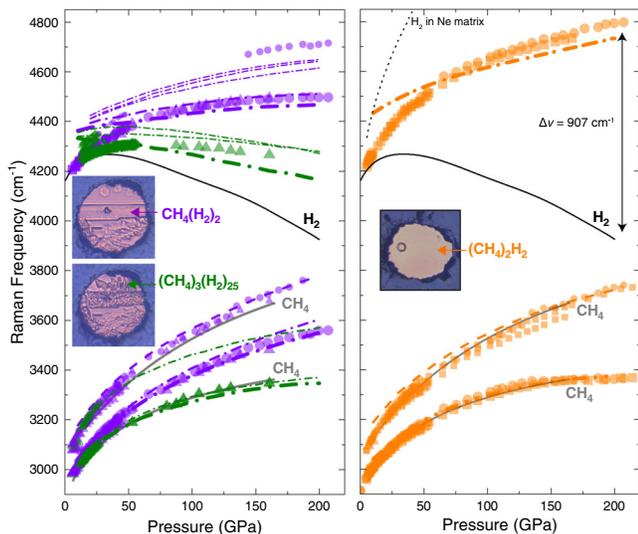
FIG. 4. Raman shift as a function of pressure of the H_2 vibrational modes and C-H stretching modes of $CH_4(H_2)_2$ and $(CH_4)_3(H_2)_{25}$ (left panel, purple and green symbols, respectively), and $(CH_4)_2H_2$ (right panel, orange symbols). Frequencies are collated from 30% (squares), 50% (circles), 70% (triangles), 80% (diamonds), and 90% (hexagons) H_2 mixtures, with the most intense modes represented by larger symbols. Raman frequencies of individual mixtures are given in Supplemental Material [45]. The dot-dashed lines represent the calculated frequencies of the H_2 modes and C-H stretching bands of each compound, with the thickest line representing the most intense modes. Black and gray solid lines represent pure H_2 [6] and CH_4 [15], respectively. The black dotted line represents the frequency of H_2 in a Ne matrix [70]. The error in pressure ranges from ± 0.2 GPa below 50 GPa, ± 1 GPa below 150 GPa, and ± 5 GPa above. The error bars in frequency are smaller than the symbol size. Photomicrographs show examples of morphology of synthesised samples within the DAC sample chamber.

Material [45]). Le Bail refinements of the experimental diffraction patterns were performed using the trigonal space group $R\bar{3}m$, which is obtained considering the carbon atoms only, and the hexagonal setting, which resulted in good fits to the data. The obtained volume per methane molecule is close to $V_{CH_4} + 8.33V_{H_2}$ (see Fig. 2), the volume of an ideal mixture of CH_4 and H_2 with the same composition. A comparison between the experimental and computational vibrational Raman modes of $CH_4(H_2)_2$-$P6_3/mmc$ and $(CH_4)_3(H_2)_{25}$-$C2/m$ is given in Fig. 4, where we see qualitatively good agreement between the number of modes, relative intensity, and frequency for both compounds.

In methane-rich concentrations of 30 mol % H_2, we observe a body-centered tetragonal Al_2Cu-type structure (space group $I4/mcm$) to form above 4.6 GPa (with $a = 7.195$ Å and $c = 5.909$ Å at 5.4 GPa), which is consistent with the previously reported composition of $(CH_4)_2H_2$ [21] (see Fig. 1). Raman spectroscopy measurements show that the CH_4 stretching bands of $(CH_4)_2H_2$ are close to the frequencies of pure solid CH_4, while two wagging modes are

observed. The number of modes and frequencies are in good agreement with our calculated values (see Fig. 4). The ν_{1H} mode, corresponding to H_2 units within the structure, exhibits the most extreme hardening of any stoichiometric molecular compound [25,28]. At a pressure of 207 GPa, $(CH_4)_2H_2$-ν_{1H} has a frequency of 4798 cm^{-1}, over 900 cm^{-1} higher than H_2-ν_1 (see Fig. 4). Remarkably, the frequencies we observe reach similar values to an impurity H_2 molecule isolated in a noble gas matrix, albeit at higher pressure [70]. Up to pressures of 207 GPa, we do not observe a turnover of ν_{1H} (and 500 GPa in our calculations), unlike in pure H_2, which exhibits a maximum frequency at approximately 38 GPa [5].

These results highlight the enormous impact that the local environment around a H_2 molecule can have on its vibron frequency. In Supplemental Material [45], we present a simple molecular model demonstrating that the vibron frequency of a H_2 surrounded by two CH_4 (respectively, H_2) will continuously increase (respectively, decrease) if the surrounding molecules are pushed closer. A molecular orbital analysis reveals that, in H_2-dominated environments, intermolecular interactions lead to occupancy of antibonding H-H σ^* states, which does not happen in CH_4-dominated environments. In $(CH_4)_2H_2$, every H_2 has two nearest H_2 neighbors and eight nearest CH_4 neighbors; as a result, the vibron exhibits extreme hardening [see Fig. 2(c) and Supplemental Material [45] for graphical representations of the unit cells and intermolecular distances]. This local environment is reversed in $(CH_4)_3(H_2)_{25}$ with an average of 9.8 H_2 neighbors but only 2.24 CH_4 neighbors per H_2 molecule; still, it remains very different from H_2-I, having a coordination number of 12 and considerably shorter H_2-H_2 distances [28]. For $(CH_4)_3(H_2)_{25}$, the ν_{1H} mode has a maximum at about 70 GPa, and the vibron frequencies tend toward the values found for pure H_2. In $CH_4(H_2)_2$, where each H_2 has six nearest H_2 neighbors and six nearest CH_4 neighbors, the vibron frequencies are interpolated between $(CH_4)_3(H_2)_{25}$ and $(CH_4)_2H_2$.

We find that the pressure-composition phase diagram is simpler than previously reported [21], with only three stable CH_4-H_2 compositions. In 50 mol % H_2 mixtures, we observe the coexistence of both $(CH_4)_2H_2$ and $CH_4(H_2)_2$, together with some excess H_2, indicative that equilibrium has not been reached. Furthermore, we observe trace amounts of $(CH_4)_3(H_2)_{25}$, which can be attributed to macroscopic inhomogeneity within the sample chamber. In 70 mol % and 80 mol % H_2 mixtures, we first observe the Raman signatures of $(CH_4)_3(H_2)_{25}$ at 14.5 GPa and at 13.6 GPa (shown as open symbols in Fig. 1), respectively, while in 90 mol % mixtures, we observe $(CH_4)_3(H_2)_{25}$ at 10.9 GPa. It is possible that, in 70 mol % and 80 mol % H_2 mixtures, formation occurs at lower pressure but is below the detection limit in the Raman spectra. We find that even in 90 mol % mixtures the transformation from $CH_4(H_2)_2$

and H_2 to $(CH_4)_3(H_2)_{25}$ is never complete, suggestive that the transformation is kinetically sluggish and due to hindered diffusion of H_2 in the solid state. Although our liquidus curve is in good agreement with that reported previously, we do not observe either CH_4H_2 and $CH_4(H_2)_4$ and attribute this to a misinterpretation of $CH_4(H_2)_2$ [21]. The experimental volume given for hexagonal wurtzite CH_4H_2 is identical to our experimental volume for $CH_4(H_2)_2$ at the same given pressure. Furthermore, after extensive structure searches, with randomly oriented molecules in the reported wurtzite center-of-mass positions, we do not find any version of the hexagonal wurtzite structure to be dynamically stable. The evidence for $CH_4(H_2)_4$ was predominantly based on Raman spectroscopy, and we find to be a misinterpretation of the coexistence between the CH_4-H_2 mixed fluid and solid $CH_4(H_2)_2$ (see Fig. S8 [45]).

$(CH_4)_3(H_2)_{25}$ possesses 51.1 wt % molecular hydrogen (63.4 wt % if the hydrogen of methane is included), which is the highest hydrogen content of any currently known stoichiometric compound. Notwithstanding the good agreement between the experimental and calculated data, $(CH_4)_3(H_2)_{25}$ represents an unusual and unique composition. All three compounds exhibit remarkable stability, with the Raman signatures of $(CH_4)_2H_2$ and $CH_4(H_2)_2$ detectable to at least 215 GPa and $(CH_4)_3(H_2)_{25}$ up to 165 GPa. We estimate the melting temperatures T_m of $(CH_4)_2H_2$ and $CH_4(H_2)_2$ using Lindemann's equation based on calculated Debye temperatures and found T_m significantly higher than molecular hydrogen at all pressures (see Supplemental Material [45]). This would imply that hydrogen mixed with methane would potentially not possess the melting line turnover that is observed in pure hydrogen [7]. Taken together in a planetary context, this could influence critical properties of planetary matter such as thermal conductivities and viscosities. In a materials science context, high Debye temperatures coupled with extremely large vibron frequencies ν_H are promising ingredients for high-T_c superconductivity—provided a reasonable density of states $N(E_F)$ at the Fermi energy. The molecular compounds described here are insulators (all remain transparent in the visible up to the highest pressures reached), but the presence of an electron or hole dopant would metallize the system, with partially charged entities $H_2^{\pm\delta}$ present. This motif, at least in calculations, can lead to T_c close to 200 K [71].

---

[*] ross.howie@hpstar.ac.cn
ross.howie@ed.ac.uk

[1] W. B. Hubbard, W. J. Nellis, A. C. Mitchell, N. C. Holmes, S. S. Limaye, and P. C. McCandless, Science **253**, 648 (1991).

[2] R. Chau, S. Hamel, and W. J. Nellis, Nat. Commun. **2**, 203 (2011).

[3] S. S. Lobanov, P.-N. Chen, X.-J. Chen, C.-S. Zha, K. D. Litasov, H.-K. Mao, and A. F. Goncharov, Nat. Commun. **4**, 2446 (2013).

[4] R. Helled and J. J. Fortney, Phil. Trans. R. Soc. A **378**, 20190474 (2020).

[5] H.-k. Mao and R. J. Hemley, Rev. Mod. Phys. **66**, 671 (1994).

[6] R. T. Howie, C. L. Guillaume, T. Scheler, A. F. Goncharov, and E. Gregoryanz, Phys. Rev. Lett. **108**, 125501 (2012).

[7] R. T. Howie, P. Dalladay-Simpson, and E. Gregoryanz, Nat. Mater. **14**, 495 (2015).

[8] P. Dalladay-Simpson, R. T. Howie, and E. Gregoryanz, Nature (London) **529**, 63 (2016).

[9] E. Gregoryanz, C. Ji, P. Dalladay-Simpson, B. Li, R. T. Howie, and H.-K. Mao, Matter Radiat. Extremes **5**, 038101 (2020).

[10] P. Loubeyre, F. Occelli, and P. Dumas, Nature (London) **577**, 631 (2020).

[11] R. M. Hazen, H.-K. Mao, L. W. Finger, and P. M. Bell, Appl. Phys. Lett. **37**, 288 (1980).

[12] H. Hirai, K. Konagai, T. Kawamura, Y. Yamamoto, and T. Yagi, Phys. Earth Planet. Inter. **174**, 242 (2009).

[13] L. Sun, A. L. Ruoff, C.-S. Zha, and G. Stupian, J. Phys. Chem. Solids **67**, 2603 (2006).

[14] L. Sun, W. Yi, L. Wang, J. Shu, S. Sinogeikin, Y. Meng, G. Shen, L. Bai, Y. Li, J. Liu, H.-K. Mao, and W. L. Mao, Chem. Phys. Lett. **473**, 72 (2009).

[15] J. E. Proctor, H. E. Maynard-Casely, M. A. Hakeem, and D. Cantiah, J. Raman Spectrosc. **48**, 1777 (2017).

[16] H. E. Maynard-Casely, C. L. Bull, M. Guthrie, I. Loa, M. I. McMahon, E. Gregoryanz, R. J. Nelmes, and J. S. Loveday, J. Chem. Phys. **133**, 064504 (2010).

[17] H. E. Maynard-Casely, L. F. Lundegaard, I. Loa, M. I. McMahon, E. Gregoryanz, R. J. Nelmes, and J. S. Loveday, J. Chem. Phys. **141**, 234313 (2014).

[18] L. J. Conway and A. Hermann, Geosciences **9**, 227 (2019).

[19] M. Peña-Alvarez, A. V. Brovarone, M.-E. Donnelly, M. Wang, P. Dalladay-Simpson, R. Howie, and E. Gregoryanz, Nat. Commun. **12**, 6387 (2021).

[20] P. Loubeyre, R. Letoullec, and J.-P. Pinceaux, Phys. Rev. Lett. **72,** 1360 (1994).

[21] M. S. Somayazulu, L. W. Finger, R. J. Hemley, and H. K. Mao, Science **271,** 1400 (1996).

[22] T. A. Strobel, P. Ganesh, M. Somayazulu, P. R. C. Kent, and R. J. Hemley, Phys. Rev. Lett. **107,** 255503 (2011).

[23] M. Somayazulu, P. Dera, A. F. Goncharov, S. A. Gramsch, P. Liermann, W. Yang, Z. Liu, H.-K. Mao, and R. J. Hemley, Nat. Chem. **2,** 50 (2010).

[24] D. K. Spaulding, G. Weck, P. Loubeyre, F. Datchi, P. Dumas, and M. Hanfland, Nat. Commun. **5,** 5739 (2014).

[25] A. K. Kleppe, M. Amboage, and A. P. Jephcoat, Sci. Rep. **4,** 4989 (2014).

[26] M. Somayazulu, P. Dera, J. Smith, and R. J. Hemley, J. Chem. Phys. **142,** 104503 (2015).

[27] E. J. Pace, J. Binns, M. Peña Alvarez, P. Dalladay-Simpson, E. Gregoryanz, and R. T. Howie, J. Chem. Phys. **147,** 184303 (2017).

[28] C. Ji, A. F. Goncharov, V. Shukla, N. K. Jena, D. Popov, B. Li, J. Wang, Y. Meng, V. B. Prakapenka, J. S. Smith, R. Ahuja, W. Yang, and H.-k. Mao, Proc. Natl. Acad. Sci. U.S.A. **114,** 3596 (2017).

[29] D. Laniel, V. Svitlyk, G. Weck, and P. Loubeyre, Phys. Chem. Chem. Phys. **20,** 4050 (2018).

[30] R. Turnbull, M.-E. Donnelly, M. Wang, M. Peña-Alvarez, C. Ji, P. Dalladay-Simpson, H.-k. Mao, E. Gregoryanz, and R. T. Howie, Phys. Rev. Lett. **121,** 195702 (2018).

[31] J. Binns, P. Dalladay-Simpson, M. Wang, G. J. Ackland, E. Gregoryanz, and R. T. Howie, Phys. Rev. B **97,** 024111 (2018).

[32] M. Ceppatelli, D. Scelta, M. Serrano-Ruiz, K. Dziubek, G. Garbarino, J. Jacobs, M. Mezouar, R. Bini, and M. Peruzzini, Nat. Commun. **11,** 6125 (2020).

[33] W. L. Mao and H. K. Mao, Proc. Natl. Acad. Sci. U.S.A. **101,** 708 (2004).

[34] W. L. Mao, V. V. Struzhkin, H. K. Mao, and R. J. Hemley, Chem. Phys. Lett. **402,** 66 (2005).

[35] Y. Liu, D. Duan, F. Tian, X. Huang, D. Li, Z. Zhao, X. Sha, B. Chu, H. Zhang, B. Liu, and T. Cui, RSC Adv. **4,** 37569 (2014).

[36] G. Saleh and A. R. Oganov, Sci. Rep. **6,** 32486 (2016).

[37] A. S. Naumova, S. V. Lepeshkin, and A. R. Oganov, J. Phys. Chem. C **123,** 20497 (2019).

[38] A. Zerr, G. Serghiou, R. Boehler, and M. Ross, High Press. Res. **26,** 23 (2006).

[39] H. Kadobayashi, S. Ohnishi, H. Ohfuji, Y. Yamamoto, M. Muraoka, S. Yoshida, N. Hirao, S. Kawaguchi-Imada, and H. Hirai, Sci. Rep. **11,** 8165 (2021).

[40] A. Kolesnikov, V. G. Kutcherov, and A. F. Goncharov, Nat. Geosci. **2,** 566 (2009).

[41] D. A. Kudryavtsev, T. M. Fedotenko, E. G. Koemets, S. E. Khandarkhaeva, V. G. Kutcherov, and L. S. Dubrovinsky, Sci. Rep. **10,** 1483 (2020).

[42] E. Snider, N. Dasenbrock-Gammon, R. McBride, M. Debessai, H. Vindana, K. Vencatasamy, K. V. Lawler, A. Salamat, and R. P. Dias, Nature (London) **586,** 373 (2020).

[43] W. Cui, T. Bi, J. Shi, Y. Li, H. Liu, E. Zurek, and R. J. Hemley, Phys. Rev. B **101,** 134504 (2020).

[44] A. F. Goncharov, E. Bykova, M. Bykov, X. Zhang, Y. Wang, S. Chariton, and V. B. Prakapenka, J. Appl. Phys. **131,** 025902 (2022).

[45] See Supplemental Material at http://link.aps.org/supplemental/10.1103/PhysRevLett.128.215702 for further methodological details and additional experimental and computational figures, which includes Refs. [46–68].

[46] E. Aprà et al., J. Chem. Phys. **152,** 184102 (2020).

[47] S. B. Ramsey, M. Pena-Alvarez, and G. J. Ackland, Phys. Rev. B **101,** 214306 (2020).

[48] V. Labet, R. Hoffmann, and N. W. Ashcroft, J. Chem. Phys. **136,** 074502 (2012).

[49] V. Labet, R. Hoffmann, and N. W. Ashcroft, J. Chem. Phys. **136,** 074503 (2012).

[50] H.-K. Mao, J. Xu, and P. M. Bell, J. Geophys. Res. **91,** 4673 (1986).

[51] Y. Akahama and H. Kawamura, J. Appl. Phys. **100,** 043516 (2006).

[52] Y. Grin, F. R. Wagner, M. Armbrüster, M. Kohout, A. Leithe-Jasper, U. Schwarz, U. Wedig, and H. G. von Schnering, J. Solid State Chem. **179,** 1707 (2006).

[53] S. Schaack, U. Ranieri, P. Depondt, R. Gaal, W. F. Kuhs, P. Gillet, F. Finocchi, and L. E. Bove, Proc. Natl. Acad. Sci. U.S.A. **116,** 16204 (2019).

[54] H. T. Stokes, D. M. Hatch, and B. J. Campbell, FINDSYM, ISOTROPY Software Suite (iso.byu.edu).

[55] H. T. Stokes and D. M. Hatch, J. Appl. Crystallogr. **38,** 237 (2005).

[56] T. Ohba, Y. Kitano, and Y. Komura, Acta Cryst. C **40,** 1 (1984).

[57] K. Ishizaki, P. Bolsaitis, and I. Spain, Solid State Commun. **15,** 1591 (1974).

[58] J. J. Gilvarry, Phys. Rev. **102,** 308 (1956).

[59] F. A. Lindemann, Phys. Z. **11,** 609 (1910).

[60] K. Refson, P. R. Tulip, and S. J. Clark, Phys. Rev. B **73,** 155114 (2006).

[61] A. Tkatchenko and M. Scheffler, Phys. Rev. Lett. **102,** 073005 (2009).

[62] G. Gao, A. R. Oganov, Y. Ma, H. Wang, P. Li, Y. Li, T. Iitaka, and G. Zou, J. Chem. Phys. **133,** 144508 (2010).

[63] S. J. Clark, M. D. Segall, C. J. Pickard, P. J. Hasnip, M. I. J. Probert, K. Refson, and M. C. Payne, Z. Kristallogr. **220,** 567 (2005).

[64] K. Momma and F. Izumi, J. Appl. Crystallogr. **44,** 1272 (2011).

[65] J. Gonzalez-Platas, M. Alvaro, F. Nestola, and R. Angel, J. Appl. Crystallogr. **49,** 1377 (2016).

[66] J. Rodríguez-Carvajal, Physica (Amsterdam) **192B,** 55 (1993).

[67] Y. Fei, A. Ricolleau, M. Frank, K. Mibe, G. Shen, and V. Prakapenka, Proc. Natl. Acad. Sci. U.S.A. **104,** 9182 (2007).

[68] C. Prescher and V. B. Prakapenka, High Press. Res. **35,** 223 (2015).

[69] P. Loubeyre, R. LeToullec, D. Hausermann, M. Hanfland, R. J. Hemley, H. K. Mao, and L. W. Finger, Nature (London) **383,** 702 (1996).

[70] P. Loubeyre, R. Letoullec, and J. P. Pinceaux, Phys. Rev. Lett. **67,** 3271 (1991).

[71] B. Chen, L. J. Conway, W. Sun, X. Kuang, C. Lu, and A. Hermann, Phys. Rev. B **103,** 035131 (2021).